Ceramics International **24** (1998) 163–173

PII: S0272-8842(96)00081-8
0272-8842/98 $19.00 + .00

Grain Growth in Synthetic and Natural Dolomas

A. T. Fonseca, J. M. Vieira & J. L. Baptista

Departamento de Cerâmica e Vidro, Universidade de Aveiro, 3810 Aveiro, Portugal

(Received 26 April 1996; accepted 26 August 1996)

Abstract: Grain growth of CaO and MgO phases during sintering of synthetic, natural and CaO-added natural dolomas was studied in the temperature range 1300–1700°C. The time exponents of the grain growth laws depend on the starting materials, processing parameters and sintering temperature, varying from 1/2 to 1/3 for the synthetic doloma, and from 1/6 to 1/3 for the natural doloma and CaO-added natural dolomas. Kuczynski's statistical model for the intermediate stage of solid state sintering was applied to the dual-phase interpenetrating microstructures of doloma, assuming that the volume fraction of the minor phase substitutes for the open porosity in the monophasic systems. The results showed that the model is applicable as a whole, provided that the relative widths of the CaO and MgO grain size distributions are considered to be proportional instead of equal. © 1998 Elsevier Science Ltd and Techna S.r.l.

1 INTRODUCTION

Microstructure development in ceramic systems has attracted a great deal of attention, determined either for theoretical or practical reasons.[1–15] The balance between densification and grain growth has long been recognized as the main factor that determines the final microstructure of the materials.[1–6,9,10,13] Existing grain growth models, which are usually applied to single-phase ceramic systems, involve assumptions regarding interfacial behaviour, grain shape and grain-boundary mobility, but they generally ignore the topological constraints of the systems.[7–9,16–18] From those, the stated models frequently predict kinetic relationships that do not fit well to the experimental results.[8] The effect of topological constraints on coarsening of biphasic ceramic systems with low mutual solid solubility has been investigated,[10,13–15,19] making evident that the second phase particles are effective against grain growth. However, in those systems that use either solid-solution or second phase additives to prevent abnormal grain growth, the effect of second phase particles depends on the dispersion degree achieved during powder processing.[13,15]

The theoretical study of the relationship between matrix grain size, time, temperature and volume fraction of second phase has been carried out on systems with low volume fractions of isolated, second phase particles.[1–4,8,10,16,17,20–22] The effects have been reviewed by Olgaard and Evans.[13] They did not find any systematic dependence of the stable grain size on the second phase particle size in calcite with added Al_2O_3 particles. This behaviour was attributed to the variations in the particle size distributions used and to the particle agglomeration effects.

There is no well established model for systems with a high volume fraction of a second phase with large particles located at three- and four-grain junctions and forming a continuous network.[15] Even the relationship between grain size and the volume fraction of the second phase is not unambiguously specfied if the second phase particles are non-randomly distributed and become segregated in grain boundaries. Zener[23] and Smith[24] studied the effect on inclusion particles on grain growth in polycrystalline materials and found that isolated spherical inclusions exert a back pressure, p, on the curved grain boundaries that is given by the coefficient of the restraining force $\epsilon = gf/r$ times the grain

boundary surface energy γ_{ss}, $p = \epsilon\gamma_{ss}$. Here g is a geometric factor, $g = 3/4$ for isolated spherical inclusions that are randomly dispersed in volume, and r is the inclusion radius.[16,17,21,23,24] The coefficient of restraining force, changes if inclusions become aggregated or preferentially segregated on grain boundaries.[10,20] It soon became evident that the simple proportionality between the constrained grain size G and the inclusion size normalized by the inclusion volume fraction, as given by the original Zener law, $G_{lim} = (4/3)r/f$, although often observed, is peculiar to some microstructural developments.[4,10,13,20] Modified relations have been sugested for ceramic materials and experimentally tested with limited sucess.[10,13,20]

The Zener effect has been assigned to stabilized microstructures in which a constant grain particle size ratio prevails during extended heating at high temperatures.[10] By enlarging the conditions where the Zener law should hold, it has been shown that a constant product, εR_c is necessary for steady-state growth of the grain size distribution when Hillert's rate equation for grain growth has the inclusion restraining back pressure of residual pores and inclusions added to the driving pressure of the curved grain boundaries.[17,21] R_c is the critical radius of the size distribution. In addition, the calculated steady-state grain size distribution of tridimensional grains closely matches the log-normal distribution when $\varepsilon R_c \cong 0.3$–$0.4$.[17]

A similar proportionality between grain size and normalized pore size was also noticed in the final stage of sintering, even though the small pores are mobile and may coalesce or dissolve as densification proceeds.[5,6] Kuczynski realizes that such proportionality exists early, before the closed porosity stage of sintering.[2] The same proportionality between the grain size, pore cross-sectional area and porosity, and the parameters of the coarsening laws and of specific surface area decreasing are often preserved throughout the full sintering run.[3,5,21,22,25,26] The changes of pore length in the intermediate stage of sintering balance the pore radius to ensure steadiness, keep εR_c constant and yield the Zener law of grain growth.[25] It makes sense to admit that any continuous second phase assemblage that fills the intergrain spacings will decrease grain growth, as does the open porosity, and restrain grain-boundary triple lines to move away from grain necks.[9]

The restraining effects of second phase additions on coarsening of ceramic refractories of MgO–CaO and MgO–Cr_3O_3 systems during liquid phase sintering have been studied previously.[11] The samples had two crystalline phases and a liquid sintering aid. The low value of the specific surface energy between different solid phases promoted mixing of the grains and direct bonding between particles of the dual-phase solid skeleton, thus improving the high temperature strength of the refractory.[11,12,14,26] The grain size of CaO underwent a five-fold decrease from the 90% CaO refractory to the composition of doloma.[11] The growth rate of each solid phase decreases as the proportion of the other phases increases.[11] The grain growth follows the $t^{1/3}$ law at high CaO volume fraction and $t^{1/4}$ at the dolomite composition.[11] The MgO grain size of each composition remained proportional to the CaO grain size, but the difference between the two grain sizes is enlarged by increasing the CaO volume content in the oxide mixture.[11] The effect is repeated in the high MgO side of the mixture and in the MgO–Cr_2O_3 system.[11] Grain growth of synthetic doloma for the temperature range 1400–1700°C follows the $t^{1/n}$ law, with $n = 5$ for CaO and $n = 6$ for MgO, the grain sizes remaining almost proportional during growth.[14] The ratio between MgO and CaO grain sizes in the synthetic doloma narrows with increasing temperature.[14]

The grain growth rate at 1650°C in a 50:50 vol% dual-phase mixture of fine Al_2O_3 and c-ZrO_2 is also severely reduced compared with that of either of the single phases.[15,27] The grain growth also follows the $t^{1/3}$ law, as in the MgO–CaO and MgO–Cr_2O_3 refractories.[15] Grains of the minor phase remained segregated, mostly along the triple lines, where the grains of the major phase met together. The restraining effects of second phases in the Al_2O_3–c-ZrO_2 interpenetrating microstructures is very strong for the first 10 vol% added, the grain size reduction accounting for more than half of the total grain size decrease that is observed in the full range of mixtures.[15,27] It then decreases to a shallow minimum of grain size, with a further two- to three-fold decrease when phases go to equal volume fractions. Similarly strong grain size refinement is observed when 7.5 vol% of fine Sb_2O_3 is added to ZnO at 1300°C.[10] Interpenetrating phase mixtures have been used in metal processing for many years to develop microstructures of refined grain sizes for superplastic forming. Their exploitation in the field of ceramics is limited.[15] The production of fine grained ceramics through the development of interpenetrating microstructures is viable when phases have limited solid solubility, the growing of the individual phases being inhibited since the long range interdiffusion of the elements of the minor phases is limited. It may eventually occur at fine grain sizes by short-circuiting of the interphase boundaries, being in any case a strong constraint to widespread growth of the major phase.

2 BACKGROUND OF KUCZYNSKI'S STATISTICAL MODELS OF SINTERING

The particle distribution width effect in the statistical treatment, applied to the grain growth when the second phase was the porosity, was derived by Wagner,[28] Hillert,[16] Oel,[29] Tomandl[30] and Kuczynski.[1–3] Unlike the former authors, the analytical approach adopted by Kuczynski for the densification and microstrutural evolution during sintering makes it possible to compare the results of the model to real systems, and to apply it to the intermediate and final sintering stages.

Kuczynski's model for the intermediate stage[1–3] assumes that the system is formed by polyhedral grains and cylindrical pores, L_v being their total length of pore per unit volume. The pore radius is statistically variable, whereas L_v is a well-determined function dependent on time. Integration of the pore size distribution function shows that the average pore size and the grain size depend on the porosity fraction, P, and the sinterability ratio, x_1. The parameter x_1, which depends on the width of the pore distribution, introduces into the integral solution the balance between the densification rate and the grain growth. When Zener's law[23,24] is introduced as the particular relationship between the grain size, G, and the specific surface area of the pores, the system evolves with time by following the general solution:[1–3]

$$(P/P_0)^n = (G/G_0)^{n/m} = (r/r_0)^{n/(m-1)} = 1 + Bt \qquad (1)$$

where P_0 is initial porosity, P is porosity at time t, G_0 is initial average grain size, G is average grain size at time t, r_0 is initial average pore radius, r is average pore radius at time t, $B(P_0, G_0, r_0, x, y, D, T)$ is a factor independent of time, D is the diffusion coefficient, T is absolute temperature, m and n are functions of x_1, x_1 is sinterability ratio, y is relative variance of pore size distribution and t is time.

The model was tested by Kuczynski,[1–3] Uskokovic *et al.*[6] and Miro and Notis[5] by using published data for several metals, oxides and halides and found to be valid for open porosity and closed porosity stages of sintering. Miro and Notis[5] also verified that the relationships between grain size, porosity and pore size obey Zener's law [eqn (2)]. The ratio PG/r becomes constant with time. It is a function of the relative width of the pore and grain size distribution. For finite widths of the size distributions, the value of Zener's constant [eqn (2)] can be expressed as the product of a factor of the pore size distribution width, y, multiplied by the ratio of pore surface area to total grain surface area of an ideal system, having sharp grain and pore size distributions and presenting the same values of the average pore surface area and grain size:

$$K(y) = P(G/r) = (1 + y)/2z' \qquad (2)$$

where $(1/z')$ is equal to the mentioned ratio.

In the final stage of sintering in the Kuczynski statement, S_vG is constant, where S_v (specific surface area of the pores) is equivalent to the condition εR_c = constant above. A feature of the sintering kinetics is that the specific surface area of pores decreases in a continuous way as $S_v \propto P$, without any noticeable transition at the onset of the closed pore stage.[22,25] By generalizing, the ratio of the specific surface area to the total grain surface area is the more general expression of the constraining force coefficient (ε) and it is constant for steady state grain growth.

The objectives of the present study were: (i) to evaluate the effect of the source of the starting materials and processing conditions on the kinetics of grain growth in systems with high volumic content of a second phase; (ii) to test the applicability of Kuczynski's statistical model to dual-phase systems of crystalline phases, in which the volume fraction of the minor phase is such that it can be made equivalent to the open porosity in the monophasic systems in sintering.

3 MATERIALS AND EXPERIMENTAL PROCEDURE

The starting materials were synthetic dolomite, natural and $CaCO_3$-added natural dolomites. The former was prepared by direct precipitation according to the Baron method.[31] The natural dolomite was from a Portuguese quarry deposit. To change the CaO/MgO volume ratio of natural dolomite, 18.7 wt% $CaCO_3$ BDH pro-analysis grade was added. Table 1 shows the chemical compositions of the synthetic and natural dolomites.

Table 1. Chemical compositions of the starting materials (wt%)

	CaO	MgO	SiO_2	TiO_2	Fe_2O_3	Al_2O_3	Na_2O	K_2O	MnO	L.O.I.
SD	30.99	21.41	‹200 ppm	‹200 ppm	‹200 ppm	‹200 ppm	0.01	0.05	‹200 ppm	47.58
ND	30.10	19.63	1.22	0.02	0.94	‹200 ppm	0.05	0.02	‹200 ppm	47.74
NDC	34.97	15.96	0.99	0.02	0.76	‹200 ppm	0.04	0.02	‹200 ppm	47.04

The natural dolomite particles are in the size range 10–90 μm, most of them with rhombohedral shape. The synthetic dolomite is composed of 20–25 μm particles of well-defined rhombohedral shape and agglomerates of smaller, 4–6 μm, particles.

Natural dolomite and natural dolomite with $CaCO_3$ addition were calcined for 1 h at 1000°C in air at atmospheric pressure. Synthetic dolomite was calcined for 5 h at different temperature/atmosphere conditions: 750°C/vacuum (6.65×10^{-3} Pa), 800°C/CO_2 (2.66×10^{3} Pa) and 850°C/CO_2 (13.33×10^{3} Pa). According DTA data, vacuum decomposition occurs in a single step, CaO and MgO being formed at the same time. The resulting doloma particles have the same external shape as those of the original dolomite. Decomposition under CO_2 atmosphere occurs in two steps, MgO being the the first to form.[32] High CO_2 pressure inside dolomite particles induces strong morphological changes on the original dolomite particle shape. The resulting dolomas' particles become more friable than those formed during vacuum decomposition.[33]

In the following text, the as-calcined powders are referred to as dolomas, namely: ND (natural doloma), NDC (natural doloma with added calcia), SD1 (synthetic doloma from vacuum-decomposed synthetic dolomite), SD2 (synthetic doloma from lower CO_2 pressure decomposition) and SD3 (synthetic doloma from higher CO_2 pressure decomposition).

The ND and NDC dolomas were unidirectionally pressed at 400 MPa and dolomas SD1–SD3 were isostatically pressed at 200 MPa. ND and NDC pressed dolomas were sintered at 1300, 1400 and 1500°C in air, using several soaking times. The SD1–SD3 dolomas were milled for 15 min. in an agate mortar, inside a glove box with N_2 atmosphere. Milled SD dolomas were isostatically pressed and sintered at 1700°C in air, for varied soaking times.

The MgO and CaO crystallite sizes of the dolomas were determined from X-ray difraction line broadening applied to the {2 0 0} crystallographic planes' reflections, using Scherrer's method.

The average grain size of sintered dolomas, with relative densities above 92% of the theoretical value, was determined on test-pieces that were polished using 8 μm and 0.25 μm diamond paste and ethanol as polishing fluid. The grain boundaries were revealed by thermal etching at temperatures 10–15% lower than those used in sintering. The etching time ranged from 1 to 30 min. The microstructural studies were carried out using scanning electron microscopy (SEM) in the back scattered electron image mode to identify the MgO and CaO phases, and/or secondary electron image mode to reveal the grain boundaries. The average CaO and MgO grain sizes were determined on SEM micrographs by the intercept chord method by counting more than 300 intecepts for each average size value.

4 RESULTS AND DISCUSSION

4.1 CaO and MgO grain growth

Figure 1 shows compositional heterogeneities inside dolomite particles. This feature is common to either natural dolomite or synthetic dolomite. Figure 2 shows the effect of different calcining conditions on particle morphology. Calcination of the synthetic dolomite at 750°C in vacuum (a single decomposition step) preserved the original particle shape. Calcined powders in the temperature range 800–1000°C (two decomposition steps) have irregularly shaped and friable agglomerates. The effect of hard agglomerates on densification behaviour was reported previously.[34]

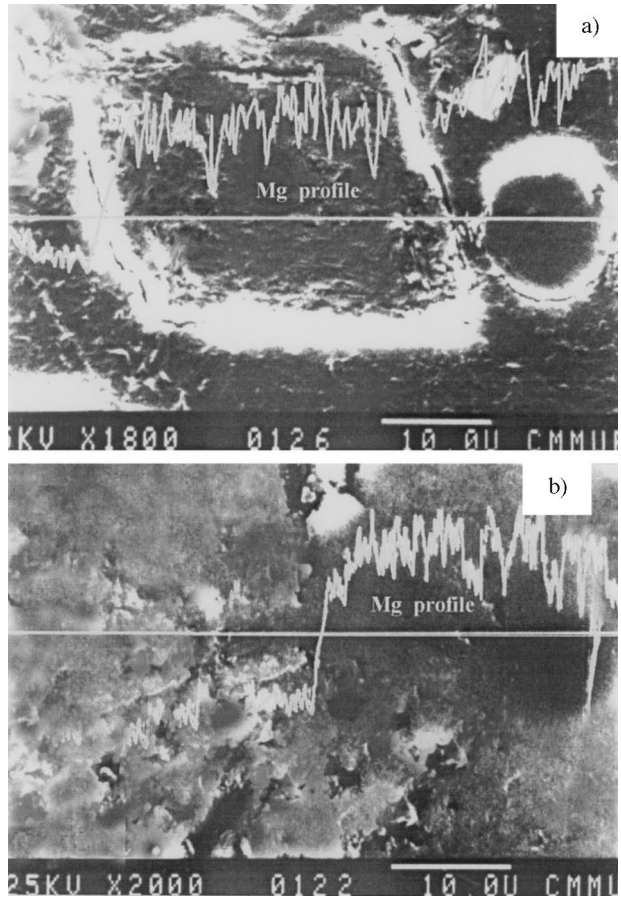

Fig. 1. Chemical heterogeneities in (a) synthetic and (b) natural dolomite with magnesium profile.

Figures 3, 4 and 5 show the kinetics of grain growth of CaO and MgO in the investigated dolomas. The time exponents of the CaO and MgO grain growth laws, $G^p - G_o^p = Ct$, depend on the starting materials, processing and sintering temperature. The values of the exponent $(1/p)$ are between 1/2 and 1/3 in SD1–SD3 dolomas and between 1/6 and 1/3 in ND and NDC dolomas. Figure 3 shows that the lower CO_2 pressure favours the grain growth of both CaO and MgO phases, which attain higher values in the SD1 material. The growth laws of the ND and NDC are quite similar, having basically the same time dependence at each sintering temperature (Figs 4 and 5).

Figure 6 shows the relationship between G_{CaO} and G_{MgO} in the SD1–SD3, ND and NDC dolomas. In the synthetic dolomite, the G_{CaO}/G_{MgO} ratio is higher in SD1 (1.83) than in SD2 or SD3 (1.35) dolomas. Different size ratios were already detected in the calcined materials, before sintering, namely: SD1—2.71, SD2—2.49 and SD3—2.07 (Table 2). Figure 7 illustrates the microstructural differences for different G_{CaO}/G_{MgO} ratios. The SD2 microstructure is more uniform than that of SD1. Although SD2 and SD3 presented different G_{CaO}/G_{MgO} ratios at the onset of sintering, they converged to the same ratio during sintering. The initial difference is explained by the decomposition mechanism: a single step in vacuum or two steps in CO_2 atmophere. In ND and NDC dolomas, which were calcined in air, that ratio is independent of sintering temperature (Fig. 6), becoming higher in the NDC doloma (3.39) than in the ND (2.40) doloma (Table 2). In the ND doloma, the grain size ratio was 2.36 after 3 h at the calcining temperature.

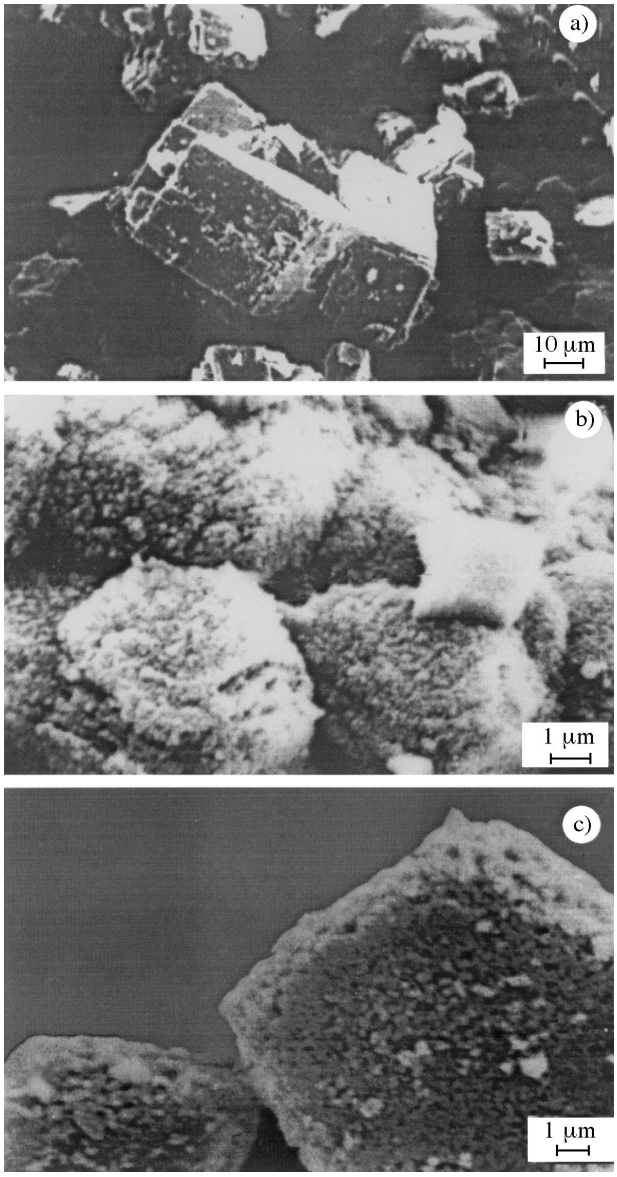

Fig. 2. Morphological aspects of the dolomas: (a) SD_1, (b) SD_3 and (c) ND.

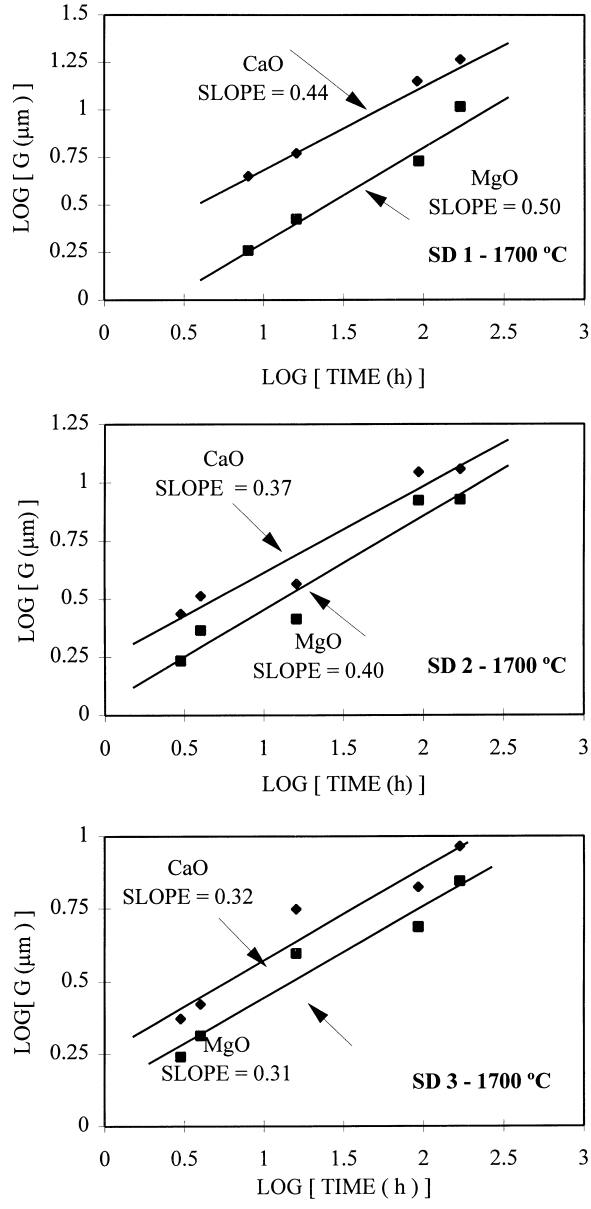

Fig. 3. Effect of the calcining conditions on the CaO and MgO grain growth in SD_1–SD_3 dolomas.

The higher value of the G_{CaO}/G_{MgO} ratio in NDC is related to the calcia-rich areas, where there are a few MgO particles. Thus, some CaO grains grow larger, contributing significantly to the high CaO average grain size. The quantity and relative statistical weight of those areas are more important in NDC than in NC. In NDC there are some pores and MgO inclusions inside CaO grains in the calcia-rich areas, the result of CaO abnormal grain growth. These MgO grains do not coalesce and grow. Abnormal grain growth can develop in a material where growth is constrained by inclusions, if the following conditions area simultaneously fulfilled:[16] the average grain size is below the limit $\varepsilon R_c < 1/2$ and there is at least one grain much larger than the average. This must be a consequence of the $CaCO_3$ addition before calcining in the present case. The MgO and CaO grain size distributions of NDC are sligtly bimodal. The effect on the Zener constant, $K(y)$, is two-fold: the abnormally large CaO grains increase the average grain size G_{CaO} and, at the same time, the size of the isolated MgO grains remains unchanged, thus the corresponding average value of G_{MgO} decreases, $K(y)$ being larger than for normal grain growth.

The phase distribution of the SD1, SD2, ND and NDC systems gives evidence (Fig. 7) of an increase in the contact surface area of the CaO–MgO phases, relative to the MgO–MgO phase contacts. This trend was also present in the early results of the CaO–MgO–liquid system,[11,12] where the values of the dihedral angle, ϕ, at the solid–solid–liquid triple lines were $\phi = 10°$ for the CaO–CaO interface, $\phi = 15°$ for MgO–MgO and $\phi = 35°$ for the

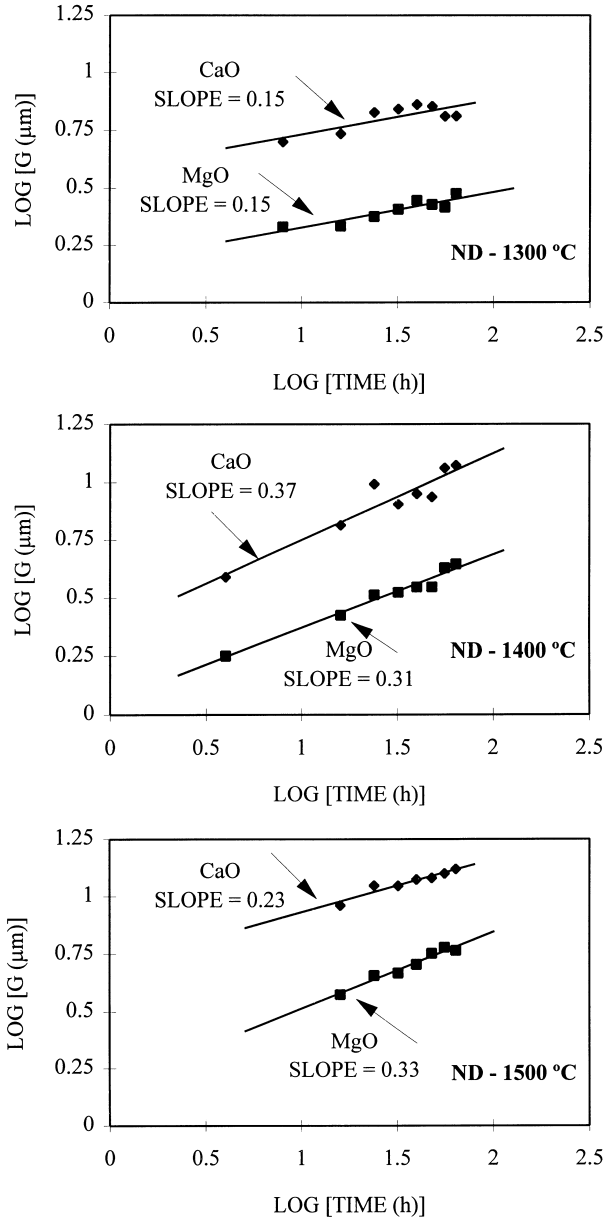

Fig. 4. Effect of sintering temperature on the CaO and MgO growth in ND doloma.

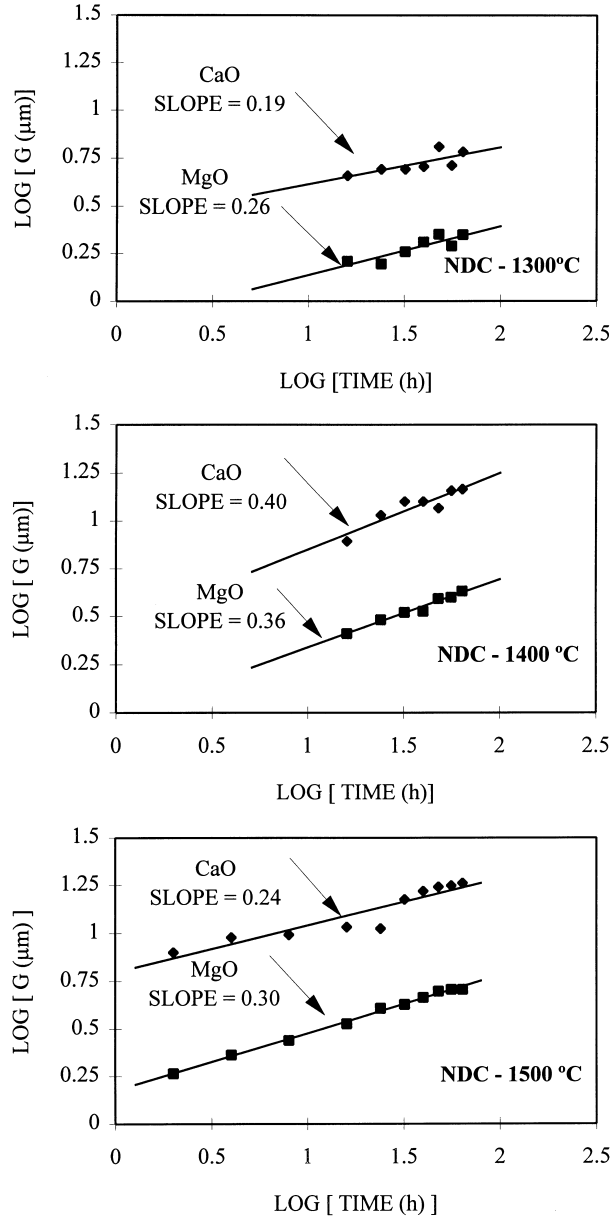

Fig. 5. Effect of sintering temperature on the CaO and MgO growth in NDC doloma.

CaO–MgO interfaces. Due to the low value of $\gamma_{CaO-MgO}$, deep necks develop at the MgO–MgO contacts (Fig. 7), and $S_{CaO-MgO}$ specific surface area is maximal.

The present results for CaO and MgO grain growth from calcined dolomites (Figs 3, 4 and 5) are different from the CaO and MgO grain growth data reported by Baldo and Bradt[14] for $Mg(HO)_2$ and $Ca(HO)_2$ calcined mixtures, with a phase volume content equal to that of the calcined dolomite. However, those authors have used very long sintering times, attaining an extremely stable microstucture with values of the grain size exponents, p, of 5 and 6 for the CaO and MgO grain growth, respectively. They attribute such stability to the topological constraints of the two phases on one another in the doloma clustered microstructure. Within experimental error, most of the values of the exponent p in Figs 3, 4 and 5 are close to $1/p = 1/3$, a value which was also observed in the 50:50 (vol%) of the Al_2O_3–c-Zr_2O system and in the CaO–MgO–liquid and MgO–Cr_2O_3–liquid systems. $1/p = 1/3$ can be identified with Ostwald ripening or to growing of interparticle necks to the critical size controlled by volume diffusion.[1,8,9,11,15,18,] The values of $1/p$ below 1/3 stand for coarsening controlled by diffusion in interphase boundaries.[9,15]

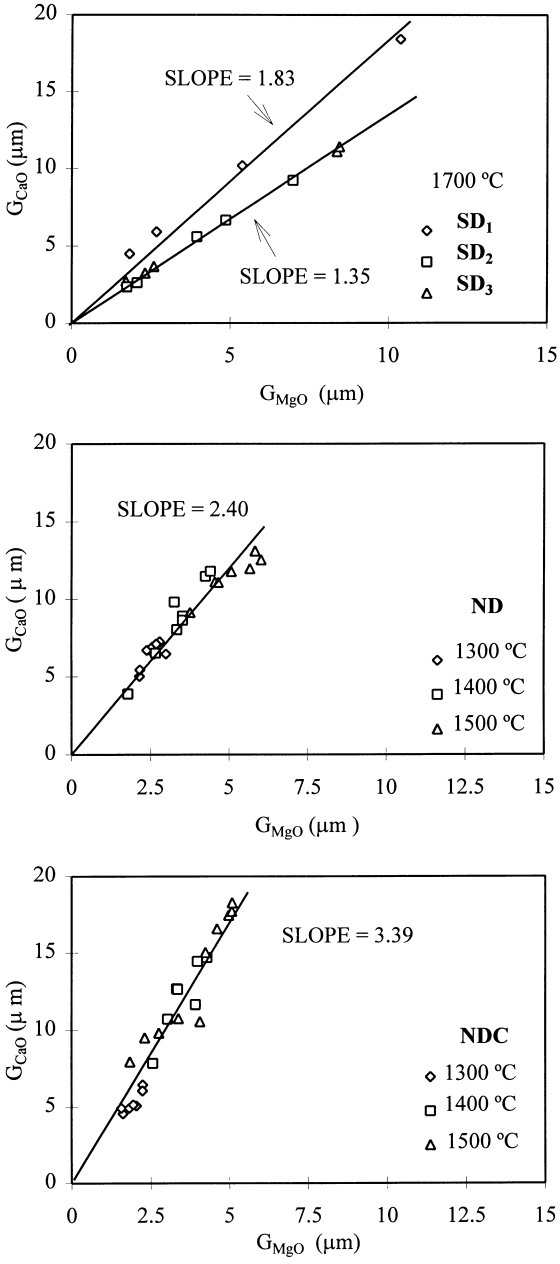

Fig. 6. Effect of the processing conditions and phase content on the G_{CaO}/G_{MgO} ratio.

4.2 Statistical analysis of grain growth

The study of the grain size distribution in ND doloma showed that the curve is asymmetric, tailed to the higher grain sizes. Figure 8 shows that the log-normal distribution can be properly fitted to the measured chord distributions.

From the approximately constant relative width of the distributions (Fig. 8 and Table 2), we conclude that the system remains almost stationary at the sintering temperature.

From the log-normal nature of the observed distributions it is possible to measure the relative widths of the distributions, the geometric variance, which is identified with the log-normal variance, and the relative variance y, the parameter that is used in Kuczynski's model, eqn (2). Figure 9 shows that the widths y and σ_{geo} are proportional, that being true for both MgO and CaO phases.

The parallelism between the straight lines of the CaO and MgO grain growth in Figs 3, 4 and 5, and the straight line joining the average CaO and MgO grain sizes in Fig. 8 for ND doloma, show that the grain sizes of the CaO and MgO phases for each type of sample are proportional, in agreement with Zener's law [eqn (2)]. The proportionality constant in ND and NDC is independent of the sintering temperature, being higher in the NDC doloma (Table 2). In the SD dolomas, the size ratio is lower than in the ND and NDC dolomas, which is due to the different origin and the sequence of decomposition mechanisms of the dolomites.

Table 2 gives the values of Zener's constant K of the ND doloma (1.1) and the NDC doloma (1.4), when the porosity in the statistical model is replaced by an equivalent porosity, the residual porosity plus the MgO volume fraction (pore sizes made comparable to MgO grain size). The values of K in Table 2 are similar to the value of K in the original Zener's equation for dispersed spherical inclusions ($K = 1.33$) and to the values that were determined for the intermediate and final stages of sintering of CoO by Miro and Notis ($K = 1.08$)[5] and of pure ZnO ($1.5 \leq K \leq 1.8$).[25]

The value of $K=1.5$ in sintering is calculated from the CaO/MgO grain size ratio of doloma sintered with 10% liquid phase.[11] The values $1.5 \leq K \leq 1.8$ in sintering of pure ZnO are related to the uniform packing of the narrow size distribution of particles in pressed compacts and they can be predicted straight from the initial values of G_0, r_0 and P_0 of the samples.[25]

The values of Zener's constant for ND, NDC and SD dolomas are not similar, even considering the correction of porosity volume fraction. However, the values are within the known ranges of K for most materials.[5,25]

These different values of Zener's constant can be attributed to the different width of the distribution curves and to the segregation degree of the MgO phase. Comparing Fig. 7(a) and (b), corresponding to SD1 and SD2, it is shown that the MgO distribution is more uniform in SD2 (two step calcation) than in SD1 (single step calcation), the former samples presenting the lowest value of Zener's constant in dolomas.

Figure 10 shows that Kuczynski's hypothesis of equal relative width of grain size and pore size distributions should be replaced by a proportionality relationship in dual-phase systems.

The constant value of the relative variance y (or σ_{geo}) of G_{CaO} and G_{MgO} in ND at each sintering temperature (Table 3) ensures that both grain size distributions remain self-similar during growth. The self-similarity is related to the steady state development of the microstructures.[17,35]

In spite of the large difference in liquid phase in the early studied MgO–CaO–liquid system[11] and the present one, that is virtually free of liquid, the values of the grain size ratio, the values of K at

Table 2. Zener's constant for the ND, NDC and SD1–SD3

	G_{CaO}/G_{MgO} (calcined)	Volume fraction (MgO+porosity)	G_{CaO}/G_{MgO} (sintered)	$(1+y)/4z'$ (calculated)
ND	2.36	0.44	2.5	2.2
NDC	—	0.39	3.5	2.8
SD1	2.71	0.47	1.9	1.8
SD2	2.49	0.45	1.4	1.3
SD3	2.07	0.45	1.4	1.3

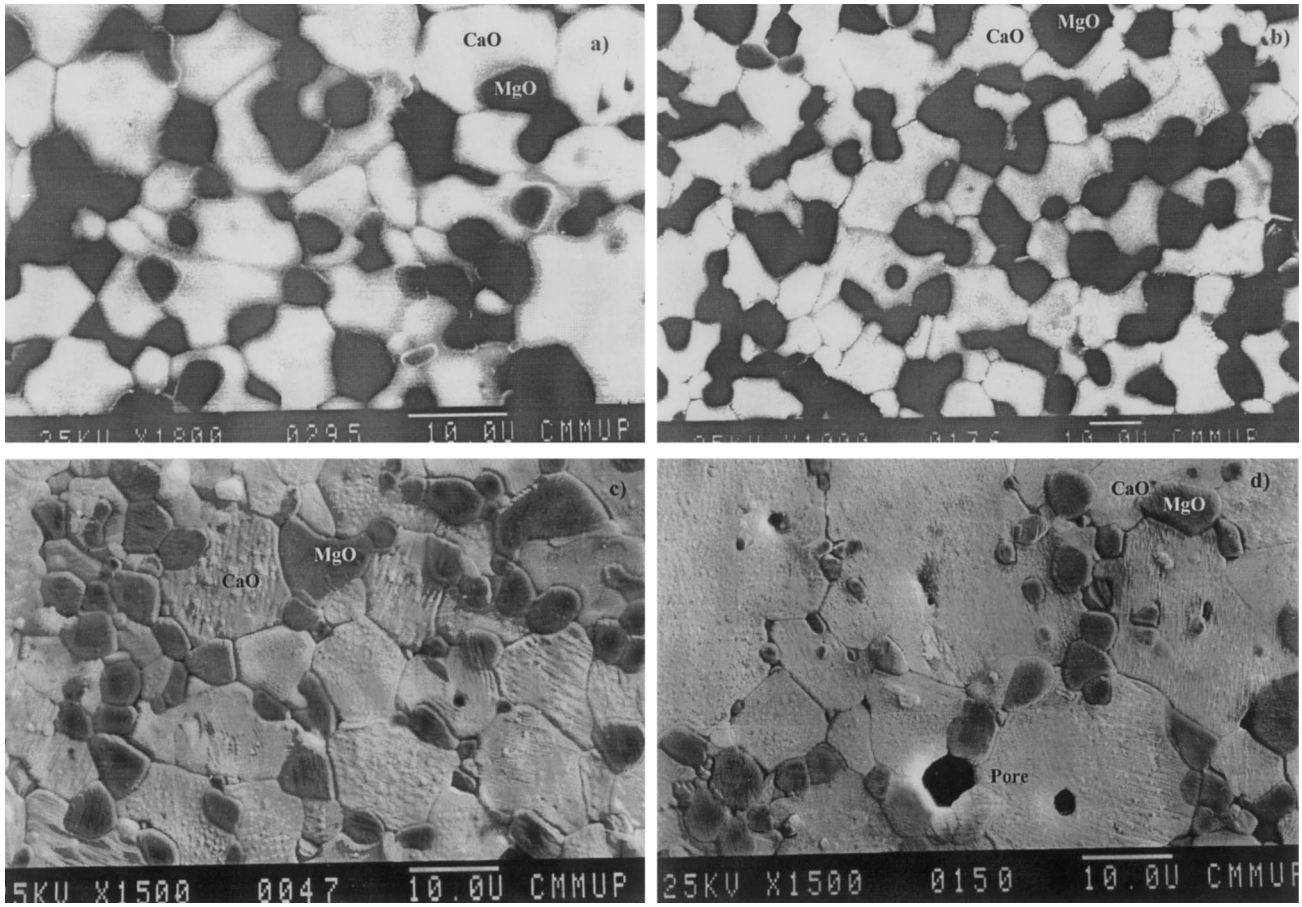

Fig. 7. Microstrutural development in dolomas: SD1 (a) and SD2 (b) fired at 1700°C for 93 h; ND (c) and NDC (d) fired at 1500°C for 64 h (darker phase — MgO).

equivalent values of CaO/MgO content, and the exponents of time of grain growth laws are close in both studies. The full range of the CaO/MgO mixture is represented in the study by White.[11] The measured values of the specific surface[11] are of the CaO–CaO interface (N_{cc}) and of the MgO–MgO interfaces (N_{mm}), for a grain size ratio below 4 these are correlated to the CaO volume fraction (f_{CaO}) and to grain size as $N_{cc} \propto f^2_{CaO}/G_{CaO}$ and $N_{mm} \propto (1-f_{MgO})^2/G_{MgO}$, respectively. These proportionalities corroborate the hypothesis that the microstructures evolved in near-equilibrium conditions of randomness.

The solution of Kuczynski's model in eqn (1), which was established by assuming steady-state evolution as given by the constant value of εR_c (or the Zener law), sets that the grain size of major phase in the dual-phase interconnected microstructures must relate to the phase volume fraction (f) as $G_f(1-f_j)^m = \text{constant}$. The following laws of

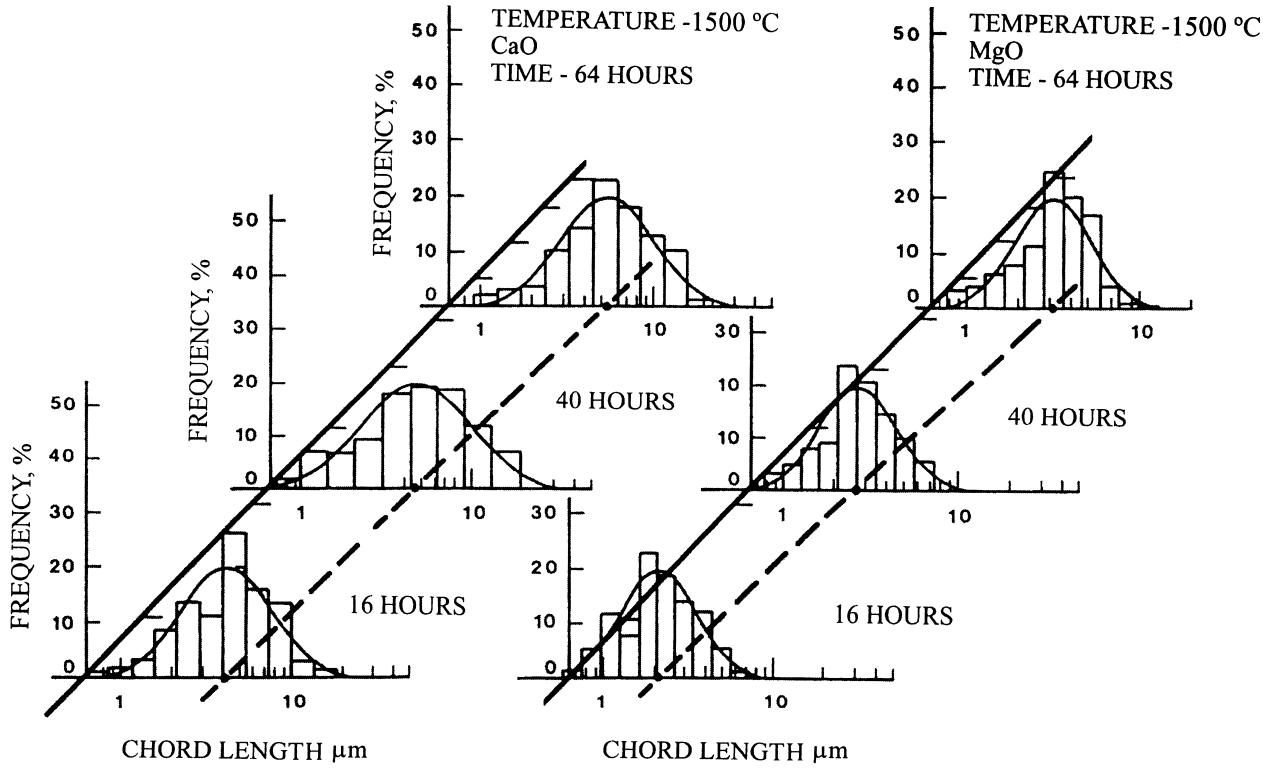

Fig. 8. Temporal evolution of CaO and MgO grain size distributions in the ND sintered at 1500°C.

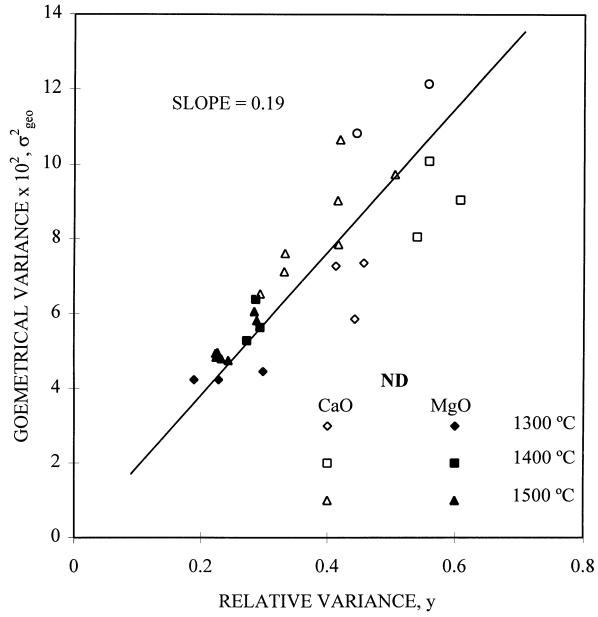

Fig. 9. Relative variance and geometrical variance relationship.

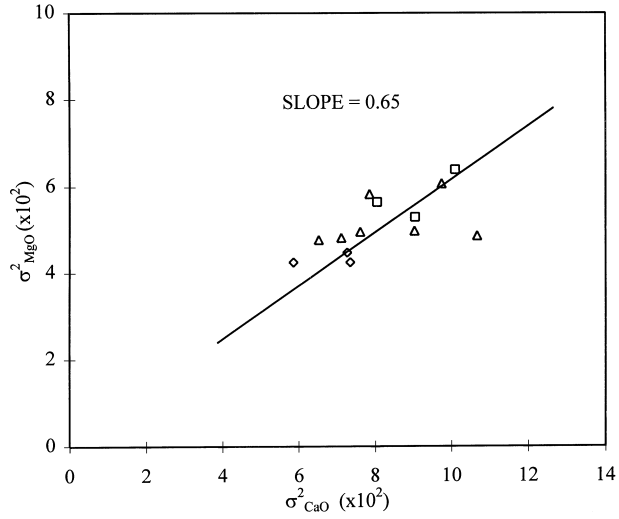

Fig. 10. Proportionality between the CaO and MgO variance of grain size distributions in ND dolomas.

Table 3. Statistical parameters of the ND and NDC microstructures

Doloma	Temperature (°C)	Time (h)	Chord length (μm)		Relative variance		Geometrical variance($\times 10^2$)	
			CaO	MgO	CaO	MgO	CaO	MgO
ND	1300	16	2.425	1.429	0.442	0.189	5.858	4.237
		40	3.205	1.454	0.456	0.228	7.350	4.237
		64	2.970	1.732	0.412	0.298	7.270	4.462
	1400	16	3.562	1.631	0.540	0.293	8.055	5.637
		40	3.801	2.107	0.608	0.272	9.045	5.285
		64	5.380	2.625	0.559	0.286	10.090	6.379
	1500	16	4.934	2.376	0.331	0.232	7.118	4.805
		24	5.665	2.822	0.293	0.243	6.525	4.759
		32	5.932	3.034	0.419	0.224	10.669	4.845
		40	5.290	3.009	0.416	0.288	7.853	5.821
		48	5.423	3.420	0.505	0.284	9.734	6.058
		56	5.544	3.590	0.415	0.226	9.027	4.965
		64	6.443	3.570	0.332	0.223	7.613	4.945
NDC	1500	16	5.788	2.250	0.558	—	—	—
		64	9.459	3.390	0.445	—	—	—

grain growth are calculated from the published[11] values of grain size of the CaO–MgO–liquid system:

$$G_{\mathrm{CaO}}(1-f_{\mathrm{CaO}})^{0\cdot 74} = C_1 0\cdot 20 \le f_{\mathrm{CaO}} \le 0\cdot 85 \qquad (3a)$$

$$G_{\mathrm{MgO}}(1-f_{\mathrm{MgO}})^{0\cdot 40} = C_2 0\cdot 30 \le f_{\mathrm{MgO}} \le 0\cdot 80 \qquad (3b)$$

The values of the exponent m in eqns (3a) and (3b) are in the range of values of the corresponding exponents of fine ZnO.[25]

Key elements of the models of grain growth constrained by the back pressure of inclusions that were previously established for isolated inclusions in low volume fractions are also found in coarsening of dual-phase interpenetrating microstructures, such as those of doloma. The bridging between the models and the present results came from Kuczynski's analysis of sintering and grain growth of solid stage sintering with open porosity. In summary, the constant value of εR_c (or $S_v G$), the observation of the Zener law and of the log-normal distribution of particles and inclusion sizes, the self-similarity of the size distributions, the exponent of time are traces of the steady state evolution of the microstructure, when dragged by the second phases in the absence of abnormal grain growth. This analysis enlarges the basis for predictable microstructure evolution of refractory binary phase mixtures and ceramic matrix composites, where fine dispersions of low solubility inclusions are incorporated or develop in the sintering of the body.

5 CONCLUSIONS

The results show important relationships between the raw material sources, powder preparation steps and the grain growth in doloma. The statistical treatment showed that Kuczynski's model holds when applied to systems with two crystalline phases, in which the minor phase is made equivalent to the immobile cylindrical pores of the intermediate sintering stage in single-phase systems. However, if the second phase is partially segregated, the changes caused in the statistical parameters need to be further investigated.

REFERENCES

1. KUCZYNSKI, G. C., Statistical approach to the theory of sintering. *Mater. Sci. Res.*, **10** (1975) 325–337.
2. KUCZYNSKI, G. C., Statistical theory of sintering. *Z. Metallkunde*, **67** (1976) 606–610.
3. KUCZYNSKI, G. C., Statistical theory of sintering and microstucture evolution. *Mater. Sci. Monog.*, **14** (1981) 37–44.
4. FANG, T.-T. & PALMOUR III, H., Useful extensions of the statistical theory of sintering. *Ceram. Int.*, **15** (1989) 1–7.
5. MIRO, A. & NOTIS, M. R., Quantitative image analysis of microstructure development during pressure sintering of CoO. *Mater. Sci. Res.*, **13** (1979) 457–469.
6. USKOKOVIC, D., PETROVIK, V. & RISTIC, M. M., Interdependence of the porosity, grain size and pore size during intermediate stage sintering. *Mater. Sci. Res.*, **13** (1979) 471–477.
7. NICHOLS, F. A., Theory of grain growth in porous compacts. *J. Appl. Phys.*, **37** (1966) 4599–4602.
8. BROOK, R. J., Controlled grain growth. In *Treatise on Materials Science and Technology*, Vol. 9, ed. F. F. Y. Wang. Academic Press, New York, 1976, pp. 331–365.
9. GRESKOVICH, C. & LAY, K. W., Grain growth in very porous Al_2O_3 compacts. *J. Am. Ceram. Soc.*, **55** (1972) 142–146.
10. KIM, J., KIMURA, T. & YAMAGUCHI, T., Microstructure development in Sb_2O_3-doped ZnO. *J. Mater. Sci.*, **24** (1989) 2581–2586.
11. WHITE, J., Phase distribution in ceramics. In *Ceramic Microstructures*, ed. R. M. Fulrath & J. A. Pask. Robert E. Krieger Publishers Co., New York, 1968, pp. 729–762.
12. WHITE, J., Phases and interfaces in ceramics. *Glass and Ceram. Bull.*, **23** (1976) 43–71.

13. OLGAARD, D. & EVANS, B., Effect of second-phase particles on grain growth in calcite. *J. Am. Ceram. Soc.*, **69** (1986) C272–C276.
14. BALDO, J. B. & BRADT, C., Grain growth of the lime and periclase phases in a synthetic doloma. *J. Am. Ceram. Soc.*, **71** (1988) 720–725.
15. FRENCH, J. D., HARMER, M. P., CHAN, H. M. & MILLER, G., Coarsening-resistant dual-phase interpenetrating microstructures. *J. Am. Ceram. Soc.*, **73** (1990) 2508–2510.
16. HILLERT, M., On the theory of normal and abnormal grain growth. *Acta Metall.*, **13** (1965) 227–238.
17. WATANABE, R. & MASUDA, Y., The effect of residual pores on the grain size distribution in sintered metal compacts. *Mater. Sci. Eng.*, **30** (1977) 33–39.
18. FISCHMEISTER, H. & GRIMVALL, G., Ostwald ripening — a survey. *Mater. Sci. Res.*, **6** (1973) 119–149.
19. WANG, J. & RAJ, R., Activation energy for sintering of two-phase alumina/zirconia ceramics. *J. Am. Ceram. Soc.*, **74** (1991) 1959–1963.
20. HAROUN, N. A. & BUDWORTH, D. W., Modifications to the Zener formula for limitation of grain size. *J. Mater. Sci.*, **3** (1968) 326–328.
21. AIGELTINGER, E. & DROLET, J. P., Third-stage sintering of carbonyl iron powder. *Modern Dev. Powder Metall.*, **6** (1974) 323–341.
22. DeHOFF, R. T., Stereological theory of sintering. In *Science of Sintering*, ed. P. Uskokovic, H. Palmour III & R. M. Spriggs. Plenum Press, New York, 1989, pp. 55–71.
23. ZENER, C., private communication.
24. SMITH, C. S., Grains, phases and interfaces: An interpretation of microstructure. *Trans. AIME*, **175** (1948) 15–51.
25. SENOS, A. M. R., Cinética de Sinterização nos Estágios de Porosidade Aberta do Óxido de Zinco, PhD Dissertation, Universidade de Aveiro, Portugal, 1993.
26. SHAW, N. J. & BROOK, R. J., Structure and grain coarsening during the sintering of alumina. *J. Am. Ceram. Soc.*, **69** (1986) 107–110.
27. FRENCH, J. D., HARMER, M. P., CHAN, H. M. & MILLER, G., Coarsening in highly interconnected microstructures. *J. Am. Ceram. Soc.*, **74** (1991).
28. WAGNER, C., *Z. Elekktrochemie*, **65** (1961) 581.
29. OEL, H. J., Crystal growth in ceramic powders. *Mater. Sci. Res.*, **4** (1969) 249–272.
30. TOMANDL, G., Statistical theory of particle growth in crystalline ceramics without liquid phase. *Mater. Sci. Res.*, **13** (1980) 61–75.
31. BARON, G., Sur la synthèse de la dolomite application au phénomène de dolomitisation. *Revue de L'Institute Français du Pétrole*, **15** (1960) 3–68.
32. POWELL, E. K. & SEARCY, A. W., Kinetics and thermodynamics of decomposition of dolomite to a metastable solid product. *J. Am. Ceram. Soc.*, **61** (1978) 216–221.
33. BERUTO, D., BARCO, L. & SEARCY, A. W., CO_2-catalyzed surface area and porosity changes in high-surface-area CaO aggregates. *J. Am. Ceram. Soc.*, **67** (1984) 512–515.
34. FONSECA, A. T., VIEIRA, J. M. & BAPTISTA, J. L., Dependence of the densification on grain growth and on agglomeration in sintering of dolomite. *J. de Physique*, **47** (1986) C1435–C1440.
35. VENKATARAN, K. S. & Di MILIA, R. A., Predicting the grain-size distributions in high-density, high-purity alumina ceramics. *J. Am. Ceram. Soc.*, **72** (1984) 33–39.